A 5×5 Microwave Permittivity Sensor Matrix in O.14-m CMOS

Hu, Zhebin; Vlachogiannakis, Gerasimos; Pertijs, Michiel A.P.; De Vreede, Leo; Spirito, Marco

DOI
10.1109/MWSYM.2018.8439438

Publication date
2018

Document Version
Accepted author manuscript

Published in
Proceedings of the 2018 IEEE/MTT-S International Microwave Symposium, IMS 2018

A 5x5 Microwave Permittivity Sensor Matrix in 0.14-µm CMOS

Zhebin Hu, Gerasimos Vlachogiannakis, Michiel A.P. Pertijs,
Leo de Vreede, and Marco Spirito
Delft University of Technology, Delft, 2628 CD, the Netherlands

***Abstract*—A 0.14-µm CMOS 2-D permittivity imaging matrix prototype operating at microwave frequencies is presented. It comprises 25 permittivity-sensing pixels, each consisting of a sensing patch connected to a dedicated RF bridge. A transconductance stage converts the imbalance voltage to a current signal, subsequently down-converted to an intermediate frequency and sampled. The implemented sensor matrix shows precise permittivity measurements over a range of 0.1-10 GHz, and successfully demonstrates permittivity contrast with a resolution of 0.1 - 2.3 from 0.1 to 10 GHz when the matrix is interfaced with various dielectrics. Owing to the matrix implementation a sub-mm, permittivity discontinuity is easily resolved by the presented sensor device.**

***Index Terms*— Bridge circuits, Chemical and biological sensors, CMOS integrated circuits, Microwave sensors, Permittivity**

I. Introduction

Miniaturized material permittivity measurements are gaining interest in various biomedical applications, including tissue and blood examination at bulk or single-cell level, in order to detect diseases and abnormalities such as cancer [1]. Although various standalone permittivity sensor implementations in CMOS technology have achieved accurate permittivity detection at GHz frequencies [2] [3], existing sensor matrixes have only been designed for frequencies below 100 MHz [4] [5]. Despite the difficulties inherent to a microwave matrix design, the incentive to move towards high-frequency broadband implementations derives from the flexibility to choose the frequency with the highest dielectric contrast, and the higher sensitivity achievable using redundant wideband data. Moreover, the matrix topology allows increased flexibility in trading-off depth of penetration versus lateral resolution, depending on the relative phases exhibited by neighboring sensing elements.

This work demonstrates, to the best of the authors' knowledge, the first CMOS microwave permittivity sensor matrix for the localized detection of permittivity variations in a material. The matrix comprises 25 individual permittivity sensing pixels that are arranged in a 5x5 rectangular matrix. Top-metal patches, utilized as dielectric sensing elements, are embedded into pixel-specific RF excited bridges and voltage-to-current conversion readout stages. The pixel excitation and readout are performed in a flexible way in order to allow multiple operation schemes such as multi-element excitation and differential readout.

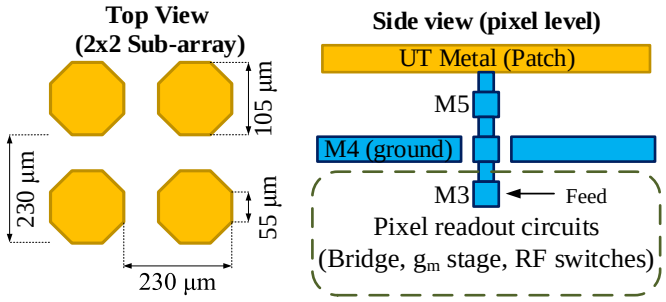

Fig. 1: Side and top view of patch within the implemented matrix.

II. System Architecture

A. Patch sensor matrix

The permittivity sensing is performed by thepatches fabricated on the top of the available 6-metals CMOS stack, with a passivation opening to achieve direct contact with the material-under-test (MUT). The patch sensors provide a permittivity dependent load admittance $Y_{L,}$ depending on both the real and imaginary part of the MUT permittivity ($\varepsilon^* = \varepsilon' - j\varepsilon''$) through a linear equation, to a first approximation, extracted from EM simulations, using Keysight EM Pro. The implementation details of the patch sensor and their arrangement in 5x5 matrix is shown in Fig. 1. To optimize compactness of the matrix, and scalability to a larger number of elements, the active detector circuits are integrated below the patch. Metal 4 is used as ground plane to isolate the patch from these active circuits. The octagonal-shape patch is connected to a M3 feed that provides access to the active drive and read circuitry through a vertical stacked via connection.

B. Matrix readout

Fig. 2 outlines the sensor matrix readout architecture. Each patch sensor is connected to a double-balanced Wheatstone bridge, using a local clipping RF driver buffer, to provide fundamental and harmonic output voltage dependent on the patch load Y_L. Differential readout is performed by means of a dummy bridge to cancel common-mode signals. As a result, the output voltage of the bridge is directly linked to the permittivity of the material interfaced to the patch. The bridge branches contain reconfigurable admittance Y_B, in the form of 4-bit binary switched capacitor control, in order to allow dynamic tuning of the bridge to the patch admittances ($Y_L \approx Y_B$). Under this condition, the bridge achieves the highest sensitivity to its load,

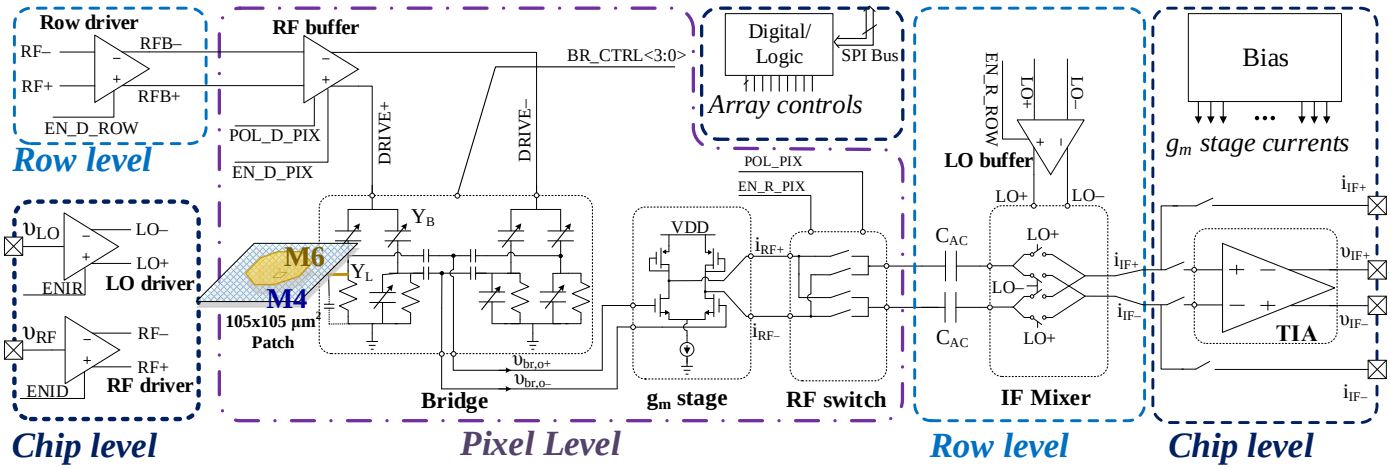

Fig. 2: Sensor matrix readout architecture.

hence permittivity, variations. This flexibility allows to vary the sensitive point of the bridge depending on the MUT's properties.

A transconductance (g_m) stage performs conversion of the bridge voltage signal to current. An RF switch is selecting any pixel output during scanning. A polarity feature in the switch is steering the pixel signal to an either in-phase or out-of-phase version of its input, equivalent to 0 or 180-degree conversion, to add differential readout functionality between pixels. Along with the enable function, polarity control is embedded also in the bridge RF buffer driver to experiment with different field distributions across the patches.

At row-level, current-mode switching down-conversion mixers translate the pixel high frequency output fundamental and harmonic currents of the corresponding row to intermediate frequency (IF) using a fast switching LO signal. The row mixer outputs are multiplexed to the output via an on-chip transimpedance amplifier (TIA) that converts the IF current to voltage and drives the chip output. A current-mode output option is also selectable for testing purposes. Input single-to-differential converters provide a differential rail-to-rail RF and LO signals which are distributed across the chip. The RF bridge drive signal is also regenerated by row drivers to achieve large drive and minimum phase imbalance conditions across the pixels. Moreover, higher harmonic components are available allowing extension of detection frequency range. The highest achievable frequency with usable resolution is bounded by the used technology node. An SPI interface is used to communicate to the chip, while digital logic allows independent access of the matrix elements. One no-patch channel with the same excitation and readout circuits is added on-chip as a reference amplitude and phase source, in order to remove amplitude fluctuations and acquire both the real and imaginary part of the output voltage. Excitation and readout of pixels can be independently enabled to allow for various reading and driving schemes to take place during material characterization. Moreover, the current mode output of the pixel signal enables multiple simultaneous current readout, performing an addition function.

III. Experimental Results

To validate the proposed architecture, the permittivity sensor was designed and fabricated in 140-nm CMOS technology. The chip size is 2.5×2.3 mm^2, with the effective sensor area of 1.15x1.15 mm^2. The sensor consumes 153mW at 900MHz from a 1.8V supply. Together with a small container, the chip was mounted on a PCB for liquid measurements (see Fig. 3), while the bonding wires were isolated from the MUT using a glob top packaging method. Six materials (de-ionized water, methanol, ethanol, 2-propanol, 1-butanol and air) are employed for complex permittivity measurement.

Fig.4 shows the output voltage amplitude of pixel 13, normalized to the reference pixel, for all bridge capacitance settings (Y_B). As shown, the bridge programmability can achieve balancing for all materials with a permittivity range from 1 (air) to 80 (water).

To calibrate every pixel of the sensor matrix for absolute permittivity versus frequency, five of the aforementioned materials were employed. Based on the linear equation and the known permittivity of five calibration materials, the expected Y_L of the patch versus permittivity were firstly estimated. Then, the offset value and coefficient of the permittivity-to-V_{out} relation were calculated by fitting the measured bridge output to a least square (LS) approximation algorithm. Fig. 5 shows the measured ε' versus pixel after calibration, when ethanol is the independent material. Moreover, three materials were separately chosen as independent materials and measured 100 times to get the standard deviation (σ) of the measurements (shown in Fig. 4). As expected, the sensor pixel achieves the lowest variation when the output amplitude is close to the minimum value. Fig.6 (a) and (b) show the average measured complex permittivity of ethanol versus frequency. The bridge can be excited with a fifth harmonic up to 10.5

GHz with a σ of lower than 0.4, shown in Fig.6(c). For the application of permittivity variation detection, the sensor achieves a resolution of 0.1-2.3 from 0.1 to 10.5 GHz, see Fig. 6(d), measured as the standard deviation of all matrix pixel measurements.

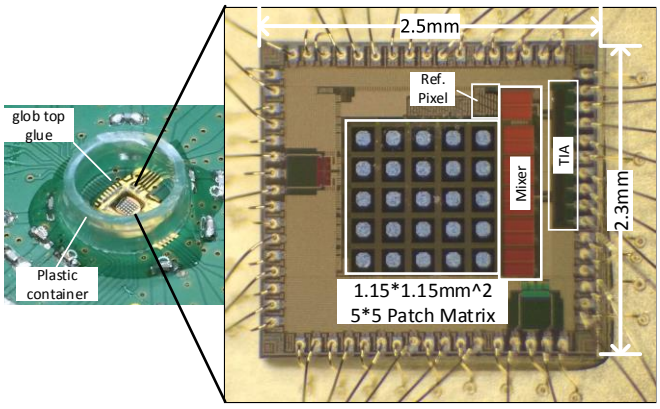

Fig. 3: Photograph of prototype chip assembling and chip micrograph.

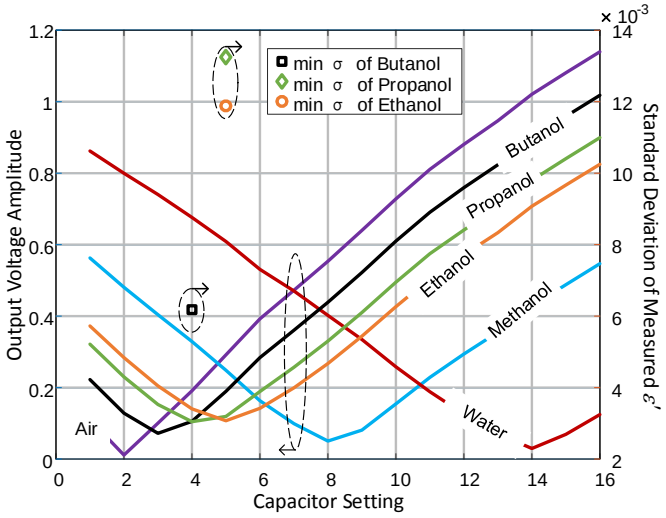

Fig. 4: Normalized output voltage amplitude of center Pixel (pixel 13) versus capacitor setting for 6 materials at 900 MHz, ant the corresponding lowest standard deviation (σ) of chosen independent material.

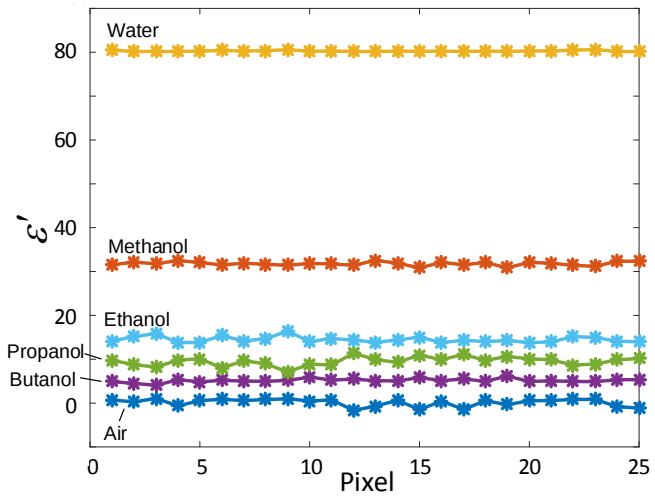

Fig. 5: ε′ of calibration and independent material (ethanol).

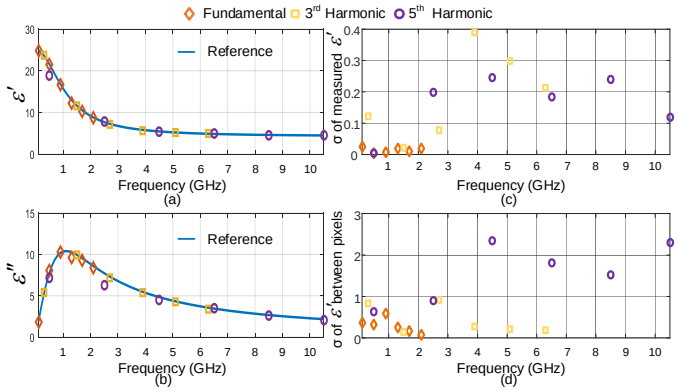

Fig. 6: Measured ethanol permittivity (real part (a) and imaginary part (b)) versus frequency, (c) σ of measured ε' and (d) σ of ε' between 25 pixels.

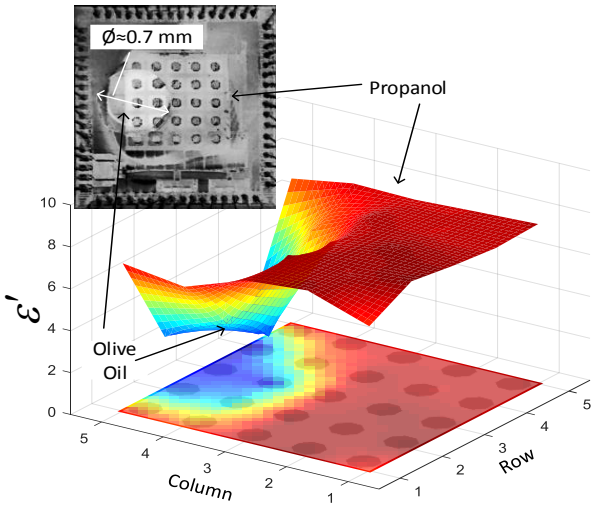

Fig. 7: Permittivity image captured by the proposed chip with different capacitor setting using MUT of propanol and olive oil at 900 MHz.

TABLE I: PERFORMANCE SUMMARY AND STATE OF THE ART

	This	[2]	[3]	[4]	[5]
CMOS node [nm]	140	180	40	350	130
Frequency	0.1-10 GHz	0.62-10 GHz	0.1-10 GHz	10-50 MHz	0.5-4 MHz
Parameter	ε′, ε″	ε′, ε″	ε′, ε″	R, C	|Z|
Power [mW]	76.5/ pixel	65-72	1-24	85	N/A
Size [mm^2]	2.5x2.3	3x3	0.15x0.3	2x2	2.2x2
Matrix (Array)	5x5	No	No	10x10	12x12
Accuracy	σ<0.4	rms error<1%	σ<0.4	N/A	N/A

Fig.7 shows the permittivity imaging result of a drop of oil inside propanol (ε′ contrast: 7.4 to 3), with a scan rate of 4 image/s, demonstrating a clear permittivity detection function. The 3D permittivity surface clearly highlights the capability of the matrix sensor to resolve a sub-mm discontinuity. Table I summarizes the performance of this chip and compares it with other works.

IV. Conclusion

This paper presents a first CMOS microwave permittivity sensor matrix. The proposed sensor shows a precise and wide range permittivity detection across a frequency range of 0.1-10.5 GHz with a compact structure. Moreover, the sensor can capture a 2-D permittivity image, for the localized detection of small permittivity variations in a material, which is suitable for non-implanted biomedical and industrial applications.

Acknowledgment

This work is supported by the Dutch Technology Foundation STW (project INFORMER 13010). The authors would like to acknowledge NXP for chip fabrication, Raf Roovers, Salvatore Drago for technical discussions, and Ali Kaichouhi for chip packaging support.

References

[1] J. Schepps and K. Foster, "The UHF and microwave dielectric properties of normal and tumour tissues: variation in dielectric properties with tissue water content", Phys. Med. Biol., vol. 25, no. 6, pp. 1149-1159, 1980.

[2] M. Bajestan, et. al "A 0.62–10 GHz complex dielectric spectroscopy system in 0.18-μm CMOS," IEEE Trans. Microw. Theory Tech., vol. 62, no. 12, pp. 3522-3537, Dec. 2014.

[3] G. Vlachogiannakis, et. al., "A 40-nm CMOS Complex Permittivity Sensing Pixel for Material Characterization at Microwave Frequencies," IEEE Trans. Microw. Theory Tech.., vol. PP, no. 99, pp. 1-16.

[4] A. Manickam, et. al., "A CMOS Electrochemical Impedance Spectroscopy (EIS) Biosensor Array," IEEE Trans. Biomed. Circ. Syst., vol. 4, no. 6, pp. 379-390, Dec. 2010.

[5] T. Chi et al., "A Multi-Modality CMOS Sensor Array for Cell-Based Assay and Drug Screening," IEEE Trans. Biomed. Circ. Syst., vol. 9, no. 6, pp. 801-814, Dec. 2015.